analytical chemistry

pubs.acs.org/ac Article

Effects of Amine Linkers with Different Carbon Chain Lengths at Guanine-Rich Polynucleotides on Chemical Interface Damping in Single Gold Nanorods

Jaeran Lee and Ji Won Ha*

Cite This: *Anal. Chem.* 2022, 94, 7100−7106 Read Online

ACCESS | Metrics & More | Article Recommendations | Supporting Information

ABSTRACT: DNA-functionalized gold nanoparticles (AuNPs) are used for various bioapplications, such as biosensor development and drug delivery. Nevertheless, no study has reported the effect of polynucleotide chains on chemical interface damping (CID), the most recently proposed plasmon damping pathway in single AuNPs. In this study, we conducted total internal reflection scattering measurements of gold nanorods (AuNRs) to reveal the CID effect induced by amine (NH_2)-linked polynucleotides (or DNA) with guanine-rich sequences through the interaction between nitrogen and Au surfaces. Additionally, we elucidated the effect of a linear hydrocarbon chain length between NH_2 and DNA (NH_2−C_n−DNA, n = 6, 12, 18, 24) on spectral changes in single AuNRs. The localized surface plasmon resonance (LSPR) linewidth increased with an increasing number of linear carbon, from 6 to 24, due to the increase in van der Waals forces. Second, the effect of the direction (5′ or 3′ ends) of DNA attachment to the AuNR surfaces on LSPR spectral changes was investigated, and there was no significant difference in LSPR wavelength and full linewidth at half-maximum shifts caused by the DNA attachment directions (5′ or 3′ ends). Third, guanine-rich DNA can fold into four-stranded secondary structures called G-quadruplexes (GQs). We demonstrated the effect of linear carbon chain length, between NH_2 and GQs, on CID in single AuNRs. Lastly, a label-free detection of DNA hybridization events on single AuNRs was demonstrated for sensing applications. Thus, we provide an insight into the effect of amine-functionalized guanine-rich DNA with different carbon chains on LSPR spectral changes, including CID in single AuNRs.

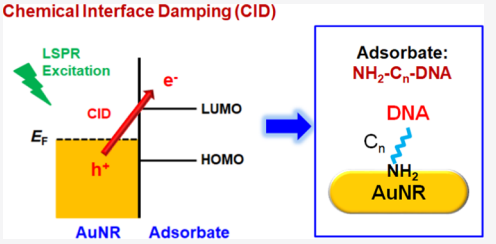

INTRODUCTION

Plasmon damping pathways on gold nanoparticles (AuNPs) are used in sensing experiments and photochemical processes.[1,2] Recently, dark-field scattering microscopy and spectroscopy have been used to investigate the broadening of homogeneous localized surface plasmon resonance (LSPR) linewidth (or plasmon damping) in single AuNPs by several groups.[3−8] Additionally, total internal reflection scattering (TIRS) microscopy and spectroscopy have been used to investigate the LSPR properties of single AuNPs.[9−11] Given the proportional relationship between the LSPR linewidth and the damping rate, the homogeneous LSPR linewidth, using far-field single-particle spectroscopy techniques, shows a detailed picture of the total LSPR decay pathway.[12,13] The LSPR linewidth is governed by lifetime broadening because of various plasmon damping channels, including bulk metal damping Γ_{bulk}, electron-surface scattering Γ_{surf}, radiation damping Γ_{rad}, and chemical interface damping (CID) Γ_{CID}.[4,8,14−18] The CID is the recently proposed damping channel pathway. In interacting adsorbate molecules, CID arises, resulting in the direct transfer of plasmon-induced hot electrons to the adsorbate's empty orbitals (LUMOs: lowest unoccupied molecular orbitals).

Single gold nanorods (AuNRs) have been mainly used to reveal the homogeneous LSPR linewidth broadening induced using the CID process with the attachment of thiolate molecules (−SH).[17−20] Nevertheless, recent studies presented the CID effect in various AuNPs, such as gold bipyramids with a sharp tip,[20] silver-coated AuNRs.[21] Additionally, recent studies have revealed that the CID effect can be caused by various adsorbate molecules, such as amine (−NH_2), pyridine, and biotinylated proteins, which have a binding affinity for AuNRs.[22] Tuning of CID in gold nanoparticles was demonstrated by controlling the electron-withdrawing and electron-donating features of adsorbate molecules and by manipulating cucurbituril-based host−guest supramolecular interactions.[13,20]

Despite the recent contributions to CID under single-particle microscopy and spectroscopy, CID is still the most unclear mechanism in plasmonic nanoparticles.[18] Additionally,

Received: March 2, 2022
Accepted: April 27, 2022
Published: May 5, 2022

https://doi.org/10.1021/acs.analchem.2c01000
Anal. Chem. 2022, 94, 7100−7106

DNA-functionalized AuNPs are used for various applications, such as biosensor development and drug delivery.[23,24] However, the effect of DNA molecules (or polynucleotide chains) as adsorbates on CID in single AuNPs has not been reported. Additionally, our understanding of the effect of linear hydrocarbon chain length, between NH_2 and DNA, on CID is limited in single AuNPs.

In this study, we measured TIRS scattering of AuNRs to understand their LSPR spectral properties at the single-particle level and to reveal CID induced by amine (NH_2)-modified DNA molecules with guanine (G)-rich sequences and different carbon chain lengths. Additionally, the effect of the direction (5′ or 3′ ends) of DNA attachment to the AuNR surfaces on LSPR spectral changes is demonstrated. Moreover, CID induced by amine-linked G-quadruplexes (GQs), having different carbon chain lengths, is presented in single AuNRs. Finally, the effect of DNA−DNA interaction (or DNA hybridization) on the LSPR of single AuNRs is presented for sensing applications.

EXPERIMENTAL SECTION

Materials and Sample Preparation. AuNRs used in this study were purchased from Nanopartz (Loveland, CO). Amine-modified DNA with a G-rich sequence was synthesized by Bioneer Inc. (Daejeon, South Korea). Potassium chloride (KCl) and the microscope cover glasses were obtained from Sigma-Aldrich (St. Louis, MO). The microscope cover glass and slide glass were cleaned by sonicating in ethanol, distilled water, and isopropanol for 15 min, successively. The solution containing the AuNRs was diluted 15 times and sonicated for 15 min to prevent the aggregation of the nanoparticles. The diluted AuNR solution was drop-casted onto the precleaned glass slide and allowed to dry. The concentration of AuNRs on the slide glass surface was controlled to be 1 μm^{-2} to characterize single AuNRs and to minimize the interparticle LSPR coupling.

Characterization of AuNRs. Structural characterizations of AuNRs were carried out using a scanning electron microscope (SEM, JSM-6500, JEOL, Japan). Furthermore, the LSPR ensemble extinction spectra of AuNRs dispersed in water were recorded with a Varian Cary 300 UV−vis spectrometer (Agilent Technologies).

Sample Preparations for Single-Particle Microscopy and Spectroscopy. The samples for single-particle studies were prepared as follows. First, the colloid AuNR solution was diluted with 18.2 MΩ pure water to proper concentration. The diluted solution was then sonicated for 10 min at room temperature. Samples were prepared by drop-casting the diluted solution onto precleaned glass slides. This slide was then covered with a 22 mm × 22 mm No. 1.5 coverslip (Corning, NY). Throughout all experiments, the area density of the AuNRs deposited on the glass slide was maintained at ∼1.0 μm^{-2} to facilitate single-particle characterization.

TIRS Microscope. The excitation of TIRS microscope was done using an inverted Nikon microscope (Nikon Eclipse Ti-2) with Halogen lamps as an excitation source. In TIRS microscopy, the beam from the halogen lamp source passed through an optical fiber with a core diameter of 100 mm. Two collimating lenses for the optical fiber were used at the opposite ends of the optical fiber. Incident light was directed into samples by a glass prism, and the incident angle was maintained at 70°. The microscope utilized a Nikon Plan Fluor oil objective (100×, NA 0.5−1.3), and the NA of the objective was maintained at 0.7. An Andor iXon^{EM} + CCD camera (iXon897) was employed to record TIRS images of AuNPs. The collected images were analyzed by ImageJ and Matlab.

TIRS Spectroscopy. Scattering spectra were acquired with a spectrometer (Andor, Kymer328i-A) and a CCD camera (Andor, Newton920). We mounted a relay lens system [a Newton lens system with two lenses (f = 7 cm)] between the microscope and the spectrometer system. The scattered light by AuNR was dispersed by grating (300 L/mm) and detected by the CCD camera. To measure the background, a region without any particles was selected. The single-particle scattering spectra of AuNRs were fitted to a Lorentzian function to measure their LSPR linewidth and the resonance peak energy.

RESULTS AND DISCUSSION

Structural characterization was conducted using scanning electron microscopy (SEM). Figure S1 shows an SEM image of AuNRs used in this study, having an average length and diameter of 74.4(±7.1) and 30(±2.1) nm, respectively (Figure S2A). The corresponding aspect ratio (AR) of AuNRs was 2.5(±0.3) (Figure S2B). The extinction spectra of the AuNR particles dispersed in water were collected using a Varian Cary 300 UV−vis spectrophotometer (Figure S3). The transverse LSPR peak appeared at ∼516 nm; the longitudinal LSPR peak appeared at 692 nm for the AuNRs. Nevertheless, single-particle measurements are used to gain an insight into the optical properties of AuNRs without ensemble averaging.

In this study, we conducted TIRS measurements of AuNRs at the single-particle level. Figure S4 shows the diagram of the experimental arrangement for TIRS studies. We investigated the effect of CID, induced by the presence of strongly interacting adsorbate molecules, on single AuNRs. The binding between sulfur or nitrogen atoms and AuNRs, with their preferred and strong covalent soft−soft bonding, has been used in CID studies.[16,19,22,25−28] In these chemical processes, interacting adsorbate molecules induce the direct generation of hot electrons for the empty LUMOs of the adsorbate (Figure 1).[29−32] The LSPR spectral frequency is red-shifted and suffers intensity loss and broadening of the full linewidth at half-maximum (FWHM).[17,18,33,34]

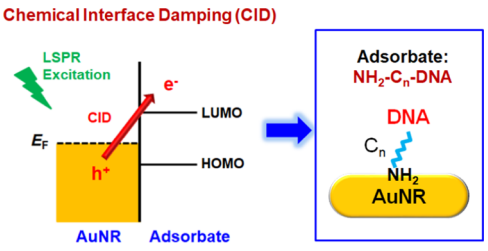

Figure 1. Schematic to show the occurrence of CID in single AuNRs upon LSPR excitation. Hot electrons generated in Au are transferred to the empty orbital LUMO of the adsorbate. The adsorbate, NH_2−C_n−DNA, used in this study is chemisorbed onto the AuNR surface through a strong Au−nitrogen interaction.

To date, the CID effect using DNA (or polynucleotides) as the adsorbate has not been demonstrated in single AuNRs. Hence, we applied amine-functionalized DNA (NH_2−DNA) as the adsorbate since the amine group can have the preferred soft−soft interactions (or dative covalent bonds) between nitrogen atoms and gold surfaces (Figure 1).[21,22,35,36] Never-

https://doi.org/10.1021/acs.analchem.2c01000
Anal. Chem. 2022, 94, 7100−7106

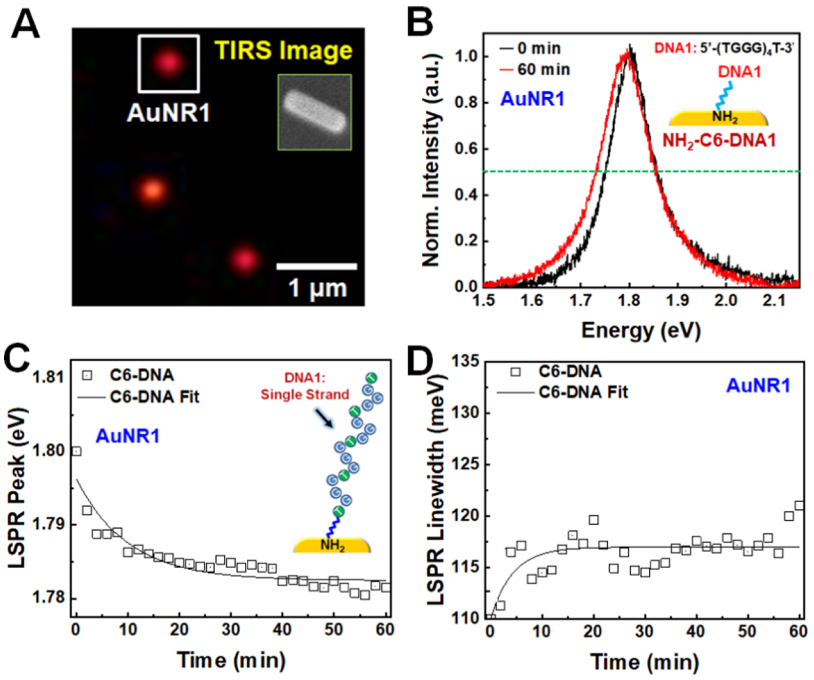

Figure 2. (A) TIRS image of single AuNRs and the inset show an SEM image of AuNR1. (B) Single-particle scattering spectra of AuNR1 before and 1 h after the chemisorption of NH_2-C_6-DNA1. DNA1 has a G-rich sequence of 5′-TGGGTGGGTGGGTGGGT-3′. (C) Time-dependent change in the LSPR peak wavelength over time at 3 min intervals after the addition of NH_2-C_6-DNA1 at 1 μM concentration. (D) Corresponding change in the LSPR linewidth over time at 3 min intervals after the addition of NH_2-C_6-DNA1 at 1 μM concentration.

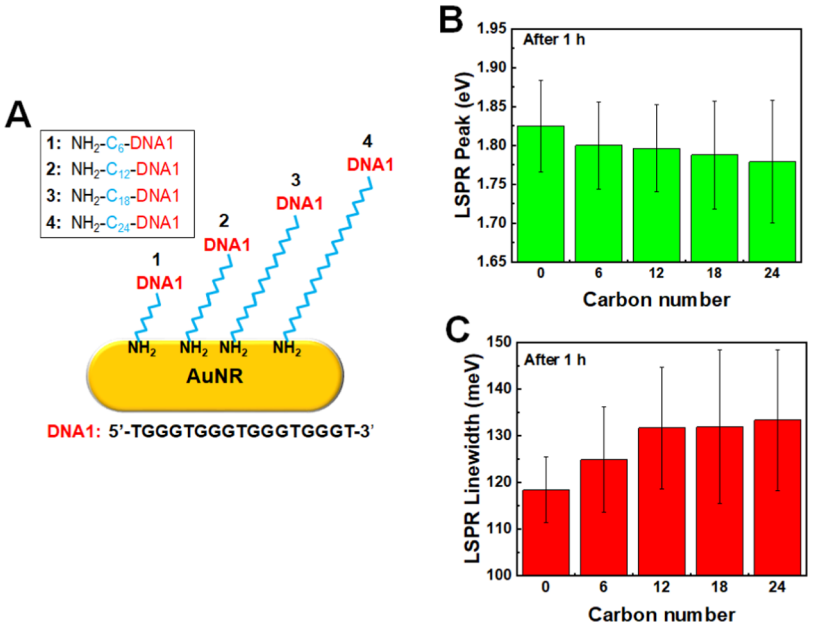

Figure 3. (A) Schematic showing the interaction between AuNR and NH_2-C_n-DNA1 with different carbon chain lengths (C_n: C_6, C_{12}, C_{18}, C_{24}). (B) Bar graph to show the comparison of LSPR peak wavelength 1 h after the chemisorption of NH_2-C_n-DNA1 (C_n: C_6, C_{12}, C_{18}, C_{24}) at 1 μM concentrations in water onto the AuNR surfaces. (C) Bar graph compares LSPR linewidth 1 h after the chemisorption of NH_2-C_n-DNA1 (C_n: C_6, C_{12}, C_{18}, C_{24}) in water onto the AuNR surfaces.

theless, to facilitate the adsorption of NH_2-DNA onto AuNR surfaces, the capping material, CTAB, on the nanoparticle surfaces was removed *via* oxygen plasma treatment.[21,37] Additionally, we used linear hydrocarbon chains of different lengths, between NH_2 and DNA (NH_2-C_n-DNA, n = 6, 12, 18, 24), to investigate the effect of chain lengths on spectral variations (LSPR wavelength shift, LSPR linewidth broadening, or CID) in single AuNRs (Figures 1 and S5).

First, we confirmed the adsorption of NH_2-C_n-DNA on single AuNRs through Au−nitrogen interaction and employed DNA1 with a G-rich sequence (5′-TGGGTGGGTGGGTGGGT-3′). Figure 2A shows a TIRS scattering image of single AuNRs deposited on a glass slide, and the inset shows an SEM image of AuNR1 obtained from a single-particle correlation study. We obtained the LSPR scattering spectra of an AuNR1 at 3 min intervals after adding

https://doi.org/10.1021/acs.analchem.2c01000
Anal. Chem. 2022, 94, 7100−7106

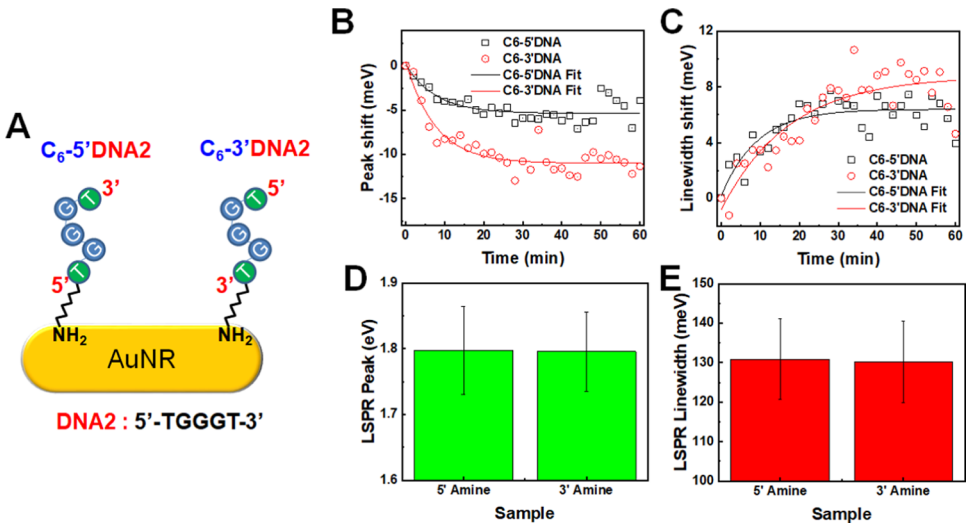

Figure 4. (A) Schematic to show the interaction of both the 5′-NH_2- and 3′-NH_2-modified single-stranded DNA molecules with the AuNR surface. (B) Time-dependent change in the LSPR peak wavelength over time at 3 min intervals after the addition of NH_2−C_6−DNA2 at 1 μM concentration. DNA2 has a short sequence of 5′-TGGGT-3′. (C) Corresponding change in the LSPR linewidth over time at 3 min intervals after the addition of NH_2−C_6−DNA1 at 1 μM concentration. (D) Bar graph compares LSPR peak wavelength 1 h after the chemisorption of both NH_2−C_6−5′DNA2 and NH_2−C_6−3′DNA2. (E) Bar graph compares the corresponding LSPR linewidth 1 h after the chemisorption of both NH_2−C_6−5′DNA2 and NH_2−C_6−3′DNA2.

an aqueous solution of NH_2−C_6−DNA1. Figure 2B shows single-particle scattering spectra of AuNR1 before and after 1 h of the adsorption of NH_2−C_6−DNA1 on the AuNR surface in water.[17,18,21,22,36] Figure 2C,D shows the time-dependent change in the LSPR wavelength and linewidth of AuNR1 after adding NH_2−C_6−DNA1 at 1 μM concentration. We observed that the LSPR wavelength was red-shifted over time for AuNR1, indicating the effective adsorption of the adsorbate. Similarly, the FWHM shift increased over time with the addition of NH_2−C_6−DNA1 (Figure 2D), indicating the occurrence of CID caused by the adsorbate on single AuNRs. Figure S6 shows the shifts of LSPR wavelength and linewidth for AuNR2 upon the adsorption of NH_2−C_{18}−DNA1 at 1 μM concentration. The same tendency was observed for NH_2−C_{18}−DNA1 having three times longer carbon chain lengths than NH_2−C_6−DNA1.

To better understand the CID effect induced by NH_2−C_n−DNA1 with different carbon chain lengths, we conducted a statistical analysis using 40 more AuNRs measured for each sample (C_0-bare, C_6, C_{12}, C_{18}, C_{24}) under the same experimental conditions (Figure 3A). Figures 3B and S7 compare LSPR peak wavelength shifts 1 h after the chemisorption of NH_2−C_n−DNA1 (C_n: C_6, C_{12}, C_{18}, C_{24}) in water onto the AuNR surfaces. The LSPR wavelength shift increased with an increase in the number of linear carbon, from 6 to 24 in single AuNRs. Additionally, as shown in Figures 3C and S8, we found that the FWHM shifts increased with increasing linear chain length, from C_6 to C_{24}, which is consistent with the result for single Au nanoparticles using 1-alkanethiol with different carbon chain lengths.[19,38] The results can be explained by the increase in van der Waals forces with increasing linear hydrocarbon chains. The effect of chemical nature on CID is further supported by previous studies.[2,20] This study is the first to present the occurrence of CID induced by NH_2−C_n−DNA1 and to verify the effect of linear carbon chain length (C_n) on the CID in single AuNRs.

The amine group can be modified at either the 5′ or 3′ ends of single-stranded DNA molecules, and both the 5′-NH_2- and 3′-NH_2-modified single-stranded DNA molecules can be adsorbed onto the AuNR surfaces (Figure 4A). In this regard, we aimed to elucidate how the 5′-NH_2- and 3′-NH_2-modified single strands chemisorbed on the Au surface could affect spectral variations (LSPR wavelength and linewidth) in single AuNRs. In this study, we applied both NH_2−C_6−5′DNA2 and NH_2−C_6−3′DNA2 with a short carbon chain (C_6) to verify their effect on the LSPR wavelength shift, as well as LSPR linewidth broadening (or CID) in single AuNRs, and DNA2 has a short sequence of 5′-TGGGT-3′ (Figure S9). Figure 4B,C shows the time-dependent change in the LSPR wavelength and linewidth of single AuNRs after adding either NH_2−C_6−5′DNA2 or NH_2−C_6−3′DNA2 at 1 μM concentration. The LSPR wavelength was red-shifted over time because of the chemisorption of both NH_2−C_6−5′DNA2 and NH_2−C_6−3′DNA2 (Figure 4B). Similarly, the FWHM shift increased over time with the addition of both NH_2−C_6−5′DNA2 and NH_2−C_6−3′DNA2 for single AuNRs (Figure 4C). For clearer comparison, we further performed statistical analysis with 40 more AuNRs measured for each sample (NH_2−C_6−5′DNA2 and NH_2−C_6−3′DNA2) under the same experimental conditions. As shown in Figures 4D and S10, the LSPR peak was observed at 1.797 eV for NH_2−C_6−5′DNA2, whereas the LSPR peak was observed at 1.796 eV for NH_2−C_6−3′DNA2. Additionally, the LSPR linewidths were 130.9 and 130.2 meV for NH_2−C_6−5′DNA2 and NH_2−C_6−3′DNA2, respectively, after chemisorption (Figures 4E and S10). Thus, there was no noticeable difference in the LSPR wavelength and FWHM shifts because of the direction (5′ or 3′ ends) of DNA attachment to AuNR surfaces.

It is known that G-rich DNA, such as DNA1 (5′-TGGGTGGGTGGGTGGGT-3′) used in this study (Figure S5), can fold into four-stranded, noncanonical secondary structures called GQs.[39,40] The core structure of GQ constituted the stacking of at least two G-tetrads, each formed by the quasi-coplanar association of four guanines linked by a network of eight hydrogen bonds. The guanines, forming the tetrads, coordinate some monovalent or divalent cations in

https://doi.org/10.1021/acs.analchem.2c01000
Anal. Chem. 2022, 94, 7100−7106

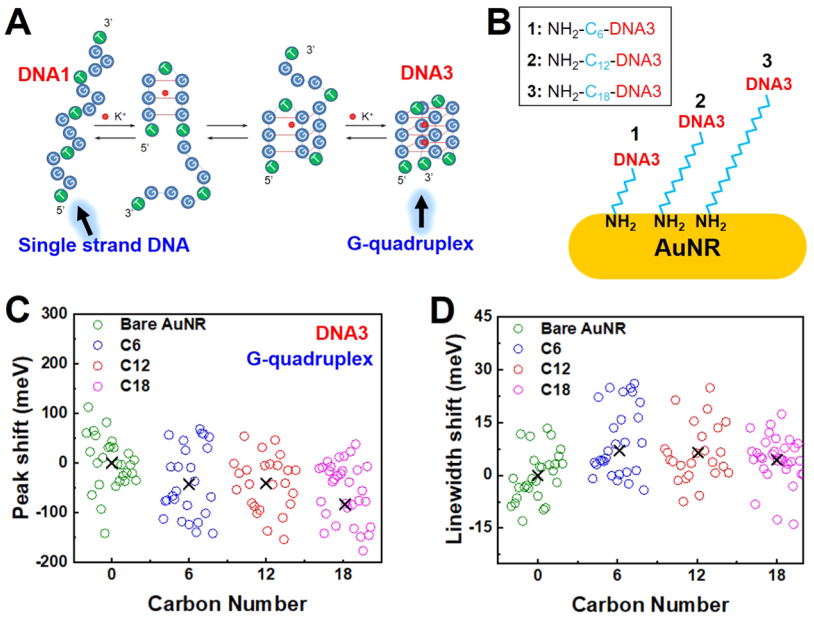

Figure 5. (A) Schematic to show folding of G-rich DNA1 (5′-TGGGTGGGTGGGTGGGT-3′) into a four-stranded secondary structure of GQ (denoted as DNA3 in this study). (B) Schematic to show the interaction between the AuNR surface and NH_2-C_n-DNA3 (C_n: C_6, C_{12}, C_{18}) at 1 μM concentrations. (C) Comparison of LSPR peak wavelength shifts 1 h after the chemisorption of NH_2-C_n-DNA3 (C_n: C_6, C_{12}, C_{18}) in water onto the AuNR surfaces. (D) Comparison of LSPR linewidth shifts 1 h after the chemisorption of NH_2-C_n-DNA3 (C_n: C_6, C_{12}, C_{18}) in water onto the AuNR surfaces.

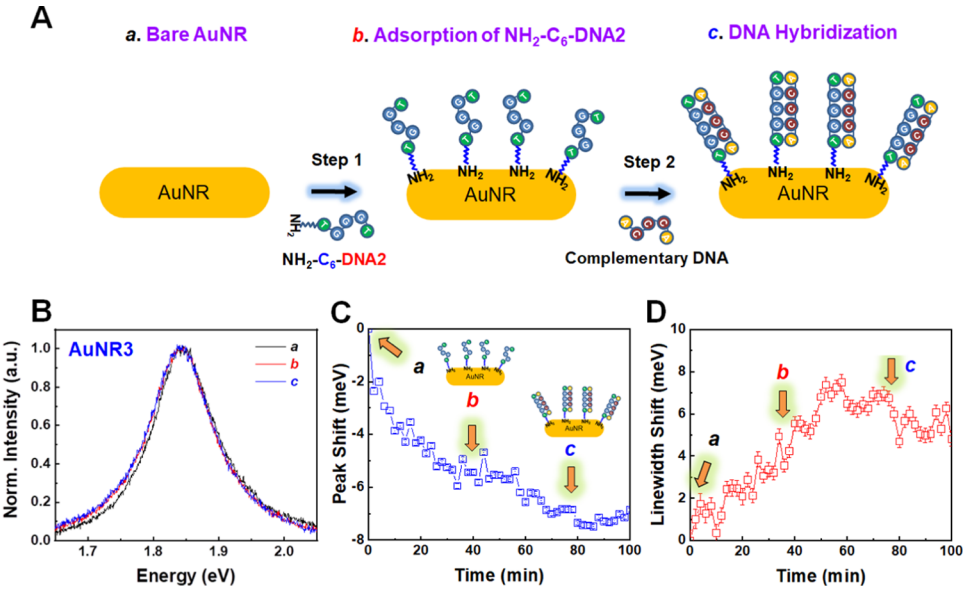

Figure 6. (A) Schematic to show the attachment of the probe DNA (NH_2-C_6-DNA2) at the AuNR surface and DNA hybridization of complementary target DNA (3′-ACCCA-5′) to the immobilized probe DNA. (B) Single-particle scattering spectra of AuNR3 before and after sequential additions of the probe DNA and complementary target DNA. (C) Time-dependent shift in the LSPR peak wavelength over time at 3 min intervals after sequential additions of the probe DNA and complementary DNA. (D) Corresponding change in the LSPR linewidth over time at 3 min intervals after sequential additions of the probe DNA and complementary DNA.

their center, typically K^+ and Na^+. Therefore, we induced structural changes from single-stranded DNA1 to GQ (DNA3) in the presence of K^+ (Figure 5A). To investigate the effect of carbon chain length on spectral changes in single AuNRs, we then used linear hydrocarbon chains of different lengths between NH_2 and DNA3 (NH_2-C_n-DNA3, n = 6, 12, 18) (Figures 5B and S11). Figure 5C compares LSPR peak wavelength shifts 1 h after the chemisorption of NH_2-C_n-DNA3 (C_n: C_6, C_{12}, C_{18}) in water onto the AuNR surfaces. As shown in Figure 5C, the LSPR wavelength shift increased with an increase in the number of linear carbon from 6 to 18 in single AuNRs, which is consistent with the result for single-stranded DNA1 in Figures 2 and 3. Furthermore, we found that the FWHM shift increased after the attachment of NH_2-C_n-DNA3 molecules (Figure 5D). However, the FWHM shift (or CID) slightly decreased (or remained almost constant within the experimental error) with increasing linear chain length from C_6 to C_{18}, and there was no significant difference

https://doi.org/10.1021/acs.analchem.2c01000
Anal. Chem. 2022, 94, 7100−7106

between the different experiments. The result could be ascribed to the presence of GQ and K^+ in the center, unlike linear single-stranded DNA1 used in Figure 3. A further theoretical calculation is necessary to explain the experimental result seen in Figure 5D.

Last, we further investigated the effect of DNA−DNA interaction on the LSPR of single AuNRs for sensing applications. More specifically, we demonstrated a label-free detection of hybridization events of nanoparticle surface-attached probe DNA (NH_2-C_6-DNA2, DNA2: 5′-TGGGT-3′) with complementary target DNA (3′-ACCCA-5′) (Figure 6A). In the first step, the single-particle scattering spectrum of bare AuNR3 fixed on a glass slide was obtained (Figure 6B, black curve), and a LSPR peak was observed at about 1.83 eV. Then, single-stranded probe DNA (NH_2-C_6-DNA2) was attached to the AuNR surface through the Au−nitrogen interaction. As a result, a red shift in the LSPR peak was observed due to a local refractive index change near the AuNR surface (Figure 6B, red curve). Afterward, the complimentary target DNA (3′-ACCCA-5′) was hybridized to the probe DNA, and additional red shift was detected due to the DNA hybridization (Figure 6B, blue curve).[41,42]

Figure 6C,D shows the time-dependent change in the LSPR wavelength and linewidth of AuNR3 after sequential additions of the probe DNA (NH_2-C_6-DNA2) and complimentary target DNA (3′-ACCCA-5′), as depicted in Figure 6A. After adding NH_2-C_6-DNA2 at 1 μM concentration, the LSPR wavelength was gradually red-shifted over time for AuNR3, indicating the effective adsorption of the adsorbate (Figure 6C). Similarly, the FWHM shift increased over time, indicating the occurrence of CID caused by the adsorbate on single AuNR (Figure 6D). In addition, after 40 min, we added the complementary DNA solution (1 μM), and DNA hybridization was observed for 1 h. As shown in Figure 6C, the DNA hybridization led to a further shift of the LSPR wavelength to longer wavelength over time for AuNR3. Moreover, additional shift in the LSPR linewidth was observed for AuNR3 due to the DNA hybridization (Figure 6D). The same tendency was further observed for AuNR4 in Figure S12. Thus, single AuNRs were demonstrated as sensing platforms to detect both the attachment of the probe DNA strands at the nanoparticle surface and the sequence-specific DNA hybridization of target DNA to the immobilized probe DNA.

CONCLUSIONS

In summary, we conducted TIRS scattering studies to understand the effect of amine-modified DNA molecules on CID in single AuNRs. Additionally, we verified the effect of a linear hydrocarbon chain length between NH_2 and DNA (NH_2-C_n-DNA, n = 6, 12, 18, 24) on LSPR spectral changes in single AuNRs. The LSPR wavelength and FWHM shifts increased with the increasing number of linear carbon from 6 to 24. The increase in FWHM shift with increasing hydrocarbon chains can be explained using the increase in van der Waals forces. Second, the effect of the direction (5′ or 3′ ends) of DNA attachment to the AuNR surfaces on LSPR spectral changes was investigated, and there was no noticeable difference in LSPR wavelength and FWHM shifts caused by the DNA attachment direction (5′ or 3′ ends). Third, G-rich DNA can fold into four-stranded, secondary structures called GQ. We elucidated the effect of linear carbon chain length between NH_2 and GQ on CID in single AuNRs. Lastly, a label-free detection of DNA hybridization events on single AuNRs was presented for sensing applications. Therefore, the results revealed the effect of amine-functionalized G-rich DNA with different carbon chains on LSPR spectral changes, including CID (or LSPR linewidth broadening) in single AuNRs.

ASSOCIATED CONTENT

Supporting Information

The Supporting Information is available free of charge at https://pubs.acs.org/doi/10.1021/acs.analchem.2c01000.

SEM image of AuNRs used in this study, their size distribution, and UV−vis spectrum; a photograph of experimental TIRS setup; chemical structures of amine-modified G-rich DNA with different carbon chain lengths; time-dependent change in the LSPR of AuNR after adding $NH_2-C_{18}-$DNA1; and time-dependent change in the LSPR of AuNR during DNA hybridization events (PDF)

AUTHOR INFORMATION

Corresponding Author

Ji Won Ha − *Department of Chemistry, University of Ulsan, Ulsan 44610, Republic of Korea; Energy Harvest-Storage Research Center (EHSRC), University of Ulsan, Ulsan 44610, Republic of Korea;* orcid.org/0000-0003-0566-8176; Phone: +82-52-712-8012; Email: jwha77@ulsan.ac.kr; Fax: +82-52-712-8002

Author

Jaeran Lee − *Department of Chemistry, University of Ulsan, Ulsan 44610, Republic of Korea*

Complete contact information is available at: https://pubs.acs.org/10.1021/acs.analchem.2c01000

Notes

The authors declare no competing financial interest.

ACKNOWLEDGMENTS

This work was supported by two National Research Foundation of Korea (NRF) grants funded by the Korean government (MSIP) (Nos. 2018R1C1B3001154 and 2019R1A6A1A11053838). Dr. Jaeran Lee also acknowledges financial support from the Basic Science Research Program of the National Research Foundation of Korea (NRF), funded by the Ministry of Education (No. 2021R1I1A1A01061317).

REFERENCES

(1) Therrien, A. J.; Kale, M. J.; Yuan, L.; Zhang, C.; Halas, N. J.; Christopher, P. *Faraday Discuss.* **2019**, *214*, 59−72.

(2) Foerster, B.; Spata, V. A.; Carter, E. A.; Sönnichsen, C.; Link, S. *Sci. Adv.* **2019**, *5*, No. eaav0704.

(3) Hu, M.; Novo, C.; Funston, A.; Wang, H.; Staleva, H.; Zou, S.; Mulvaney, P.; Xia, Y.; Hartland, G. V. *J. Mater. Chem.* **2008**, *18*, 1949−1960.

(4) Hu, M.; Petrova, H.; Sekkinen, A. R.; Chen, J.; McLellan, J. M.; Li, Z.-Y.; Marquez, M.; Li, X.; Xia, Y.; Hartland, G. V. *J. Phys. Chem. B* **2006**, *110*, 19923−19928.

(5) Novo, C.; Gomez, D.; Perez-Juste, J.; Zhang, Z.; Petrova, H.; Reismann, M.; Mulvaney, P.; Hartland, G. V. *Phys. Chem. Chem. Phys.* **2006**, *8*, 3540−3546.

(6) Wang, X.; Zhang, Z.; Hartland, G. V. *J. Phys. Chem. B* **2005**, *109*, 20324−20330.

(7) Nehl, C. L.; Grady, N. K.; Goodrich, G. P.; Tam, F.; Halas, N. J.; Hafner, J. H. *Nano Lett.* **2004**, *4*, 2355−2359.

(8) Hu, M.; Chen, J.; Marquez, M.; Xia, Y.; Hartland, G. V. *J. Phys. Chem. C* **2007**, *111*, 12558−12565.
(9) Lee, J.; Ha, J. W. *Analyst* **2021**, *146*, 4125−4129.
(10) Lee, J.; Kim, G. W.; Ha, J. W. *Analyst* **2020**, *145*, 6038−6044.
(11) Lee, J.; Kim, G. W.; Ha, J. W. *Analyst* **2022**, *147*, 1066−1070.
(12) Olson, J.; Dominguez-Medina, S.; Hoggard, A.; Wang, L.-Y.; Chang, W.-S.; Link, S. *Chem. Soc. Rev.* **2015**, *44*, 40−57.
(13) Jeon, H. B.; Park, S.; Ryu, K. R.; Ghosh, S. K.; Jung, J.; Park, K. M.; Ha, J. W. *Chem. Sci.* **2021**, *12*, 7115−7124.
(14) Sönnichsen, C.; Franzl, T.; Wilk, T.; von Plessen, G.; Feldmann, J.; Wilson, O.; Mulvaney, P. *Phys. Rev. Lett.* **2002**, *88*, No. 077402.
(15) Ha, J. W.; Sun, W.; Stender, A. S.; Fang, N. *J. Phys. Chem. C* **2012**, *116*, 2766−2771.
(16) Zijlstra, P.; Paulo, P. M. R.; Yu, K.; Xu, Q. H.; Orrit, M. *Angew. Chem., Int. Ed.* **2012**, *51*, 8352.
(17) Ha, J. W. *Chem. Phys. Lett.* **2017**, *676*, 65−69.
(18) Foerster, B.; Joplin, A.; Kaefer, K.; Celiksoy, S.; Link, S.; Sönnichsen, C. *ACS Nano* **2017**, *11*, 2886−2893.
(19) Moon, S. W.; Tsalu, P. V.; Ha, J. W. *Phys. Chem. Chem. Phys.* **2018**, *20*, 22197−22202.
(20) Lee, S. Y.; Tsalu, P. V.; Kim, G. W.; Seo, M. J.; Hong, J. W.; Ha, J. W. *Nano Lett.* **2019**, *19*, 2568−2574.
(21) Ryu, K. R.; Nam, D. H.; Lee, S.; Ha, J. W. *J. Phys. Chem. C* **2020**, *124*, 14818−14825.
(22) Moon, S. W.; Ha, J. W. *Analyst* **2019**, *144*, 2679−2683.
(23) Liu, B.; Liu, J. *Matter* **2019**, *1*, 825−847.
(24) Liu, B.; Liu, J. *Anal. Methods* **2017**, *9*, 2633−2643.
(25) Moon, S. W.; Ha, J. W. *Phys. Chem. Chem. Phys.* **2019**, *21*, 7061−7066.
(26) Paulo, P. M. R.; Zijlstra, P.; Orrit, M.; Garcia-Fernandez, E.; Pace, T. C. S.; Viana, A. S.; Costa, S. M. B. *Langmuir* **2017**, *33*, 6503−6510.
(27) Ferrier, R. C.; Lee, H.-S.; Hore, M. J. A.; Caporizzo, M.; Eckmann, D. M.; Composto, R. J. *Langmuir* **2014**, *30*, 1906−1914.
(28) de la Llave, E.; Clarenc, R.; Schiffrin, D. J.; Williams, F. J. *J. Phys. Chem. C* **2014**, *118*, 468−475.
(29) Kale, M. J.; Avanesian, T.; Christopher, P. *ACS Catal.* **2014**, *4*, 116−128.
(30) Boerigter, C.; Campana, R.; Morabito, M.; Linic, S. *Nat. Commun.* **2016**, *7*, No. 10545.
(31) Boerigter, C.; Aslam, U.; Linic, S. *ACS Nano* **2016**, *10*, 6108−6115.
(32) Seo, M. J.; Kim, G. W.; Tsalu, P. V.; Moon, S. W.; Ha, J. W. *Nanoscale Horiz.* **2020**, *5*, 345−349.
(33) Zijlstra, P.; Paulo, P. M. R.; Orrit, M. *Nat. Nanotechnol.* **2012**, *7*, 379.
(34) Lünskens, T.; von Weber, A.; Jakob, M.; Lelaidier, T.; Kartouzian, A.; Heiz, U. *J. Phys. Chem. C* **2017**, *121*, 9331−9336.
(35) Jazayeri, M. H.; Amani, H.; Pourfatollah, A. A.; Pazoki-Toroudi, H.; Sedighimoghaddam, B. *Sens. Bio-Sens. Res.* **2016**, *9*, 17−22.
(36) Hoft, R. C.; Ford, M. J.; McDonagh, A. M.; Cortie, M. B. *J. Phys. Chem. C* **2007**, *111*, 13886−13891.
(37) Kim, G. W.; Ha, J. W. *Phys. Chem. Chem. Phys.* **2020**, *22*, 11767−11770.
(38) Lee, S. Y.; Ha, J. W. *Bull. Korean Chem. Soc.* **2019**, *40*, 481−482.
(39) Spiegel, J.; Adhikari, S.; Balasubramanian, S. *Trends Chem.* **2020**, *2*, 123−136.
(40) Bochman, M. L.; Paeschke, K.; Zakian, V. A. *Nat. Rev. Genet.* **2012**, *13*, 770−780.
(41) Soares, L.; Csáki, A.; Jatschka, J.; Fritzsche, W.; Flores, O.; Franco, R.; Pereira, E. *Analyst* **2014**, *139*, 4964−4973.
(42) Schneider, T.; Jahr, N.; Jatschka, J.; Csaki, A.; Stranik, O.; Fritzsche, W. *J. Nanopart. Res.* **2013**, *15*, No. 1531.

https://doi.org/10.1021/acs.analchem.2c01000
Anal. Chem. 2022, 94, 7100−7106